Surface Patterns in Solvent-Cast Polymer Blend Films Analyzed with an Integral-Geometry Approach

J. Raczkowska,[†] J. Rysz,[†] A. Budkowski,*[,†] J. Lekki,[‡] M. Lekka,[‡] A. Bernasik,[†,§] K. Kowalski,[†,§] and P. Czuba[†]

M. Smoluchowski Institute of Physics and Joint Center for Chemical Analysis and Structural Research, Jagellonian University, Reymonta 4, 30-059 Kraków, Poland, Institute of Nuclear Physics, Radzikowskiego 152, 31-342 Kraków, and Surface Spectroscopy Laboratory, University of Mining and Metallurgy, Mickiewicza 39, 30-059 Kraków, Poland

Received June 4, 2002

ABSTRACT: Topography and composition images of model thin films of deuterated polystyrene (dPS) and polyisoprene with different blend compositions were analyzed with an extension of integral-geometry approach. Surface patterns, formed in the course of spin-casting from toluene onto self-assembled monolayers (SAM), were recorded with scanning force microscopy. Their relation with lateral phase domain structures was demonstrated by dynamic secondary ion mass spectrometry, yielding maps of dPS distribution. Morphological measures, which cannot be provided by Fourier transform analysis (FTA), characterize individual images, compositional series of the surface patterns and individual features of the patterns. Different morphologies (nucleation- and spinodal-type and hole- and island-dominated ones) are consistently characterized by the Minkowski measures and related parameters. For instance, the latter can measure circular character of the individual features and estimate dominant lateral length (determined rigorously with FTA). Lateral morphologies are hardly affected when CH_3-terminated SAM is exchanged for SAM with COOH end groups.

1. Introduction

Thin polymer blend films with well-defined surface morphologies are widely used in electronics, optics and biotechnology. Casting of homopolymer blends from a common solvent is an economical method to produce thin films with particular physical properties as well as specific patterns of surface topography. Usually the undulations at the film surface reflect the phase domain structure formed in the course of phase separation, enabled by the solvent,[1−4] a jump in temperature,[5−9] or a successive application of both these methods.[10,11] A phase separation process, qualitatively different from that in the bulk, has been studied only recently.[12−15] Specific types of formed surface patterns are requested directly by the geometry of particular application, such as antireflection coatings,[16] or regarded as a token of domain structure optimal for best device performance, as in light-emitting diodes.[17−18]

An enormous amount of information provided by surface patterns, recorded with scanning force microscopy (SFM) as topography images, has to be reduced to a finite number of relevant parameters in order to compare quantitatively different morphologies.[19] While this step has not been completed in early papers,[1,5,16−18,20−26] a minimal set of root-mean-square roughness σ_{rms} and (or) dominant length Λ values was used later to characterize vertical and lateral features of surface structures, respectively.[4,6−7,27−38] However, the Fourier transform analysis of SFM images, used to determine Λ, does not give the information about the morphology of surface patterns, i.e., their content (surface fractional coverage), shape (curvature of distinct surface features), and connectivity (density of the features). The importance of some of these parameters was soon recognized. Surface coverage was determined in refs 2, 39, and 40, feature density in ref 39, and feature size in refs 2, 40, and 41 (and in refs 42−43 for optical microscopy data). At the same time, the integral-geometry image analysis has provided means to characterize all of these surface pattern parameters in a frame of one approach using a complete set of morphological measures, provided by Minkowski functionals.[19,44−45] The integral-geometry quantities were, however, mainly used to describe phase separating and ordering bulk systems.[44,46−49] Only recently, Gutmann et al. in their seminal paper[3] have analyzed individual SFM images of surface patterns in terms of three Minkowski measures plotted as a function of height.

In this paper, we present an extension of the earlier integral-geometry approach,[3] allowing us, for the first time, to compare quantitatively surface patterns of polymer blend films using a complete set of morphological measures. First, we propose a simple method to specify, for each SFM image, characteristic values of three Minkowski functionals and compare them with those of concentration maps (see section 3.2). Then, we use these values to describe series of surface patterns formed by model film blends with varied relative fraction of blend components (section 3.3). Minkowski measures are shown not only to characterize, in a consistent way, all patterns and the transition from hole- to island-dominated morphologies but also to describe essential properties of individual dominant surface features and to define lateral length scales complementary to the dominant length Λ (section 3.4). The virtues of the integral-geometry approach are demonstrated for topographic and compositional maps (introduced in section 3.1) of two series of model polymer

* Corresponding author. E-mail: ufbudkow@cyf-kr.edu.pl. Fax: ++48-12-633 70 86. Telephone: -632 48 88.
[†] Jagellonian University.
[‡] Institute of Nuclear Physics.
[§] University of Mining and Metallurgy.

10.1021/ma020870w CCC: $25.00
Published on Web 03/11/2003

blend films. Two film series are formed by deuterated polystyrene (dPS) and polyisoprene (PI) blends[24,50,52] with different compositions, cast from toluene onto Au substrates covered with two types of self-assembled monolayers (SAM). Information provided by the integral-geometry approach can verify hypotheses on morphology formation in these solvent-cast polymer blend films (as summarized in section 4).

2. Experimental Section

2.1. Preparation of Polymer Blend Films. Au surfaces covered with SAM composed of thiols were used as the substrates. Au layers (∼50 nm thick) were evaporated onto Si wafers. To produce hydrophobic (surface energy $\gamma \sim 20$ mJ/m^2,[53] denoted later as CH_3−SAM) or hydrophilic (γ∼81 mJ/m^2,[53] denoted as COOH−SAM) substrates, the Au surfaces were rinsed with ethanol and then exposed for 60 s to ethanol solutions of 1-hexadecanethiol [$HS(CH_2)_{15}CH_3$] or 16-mercaptohexadecanoic acid [$HS(CH_2)_{15}COOH$], respectively.[53−54] Afterward, the substrates were rinsed again with ethanol and dried. Just before casting, dry substrates were flushed with fresh toluene. Then thin films were prepared by spin-casting (5550 rpm for 30 s) a toluene solution of polymer mixture (constant total polymer concentration of 20 mg/mL was used) onto the substrates, resulting in films with average thickness $d \sim 169(10)$ nm (see also ref 24). This thickness value, determined with SFM[22,38] for symmetric blends, is in accord with $d = 170(15)$ nm yielded by dynamic secondary ion mass spectrometry (SIMS).[52] To ensure complete dissolution, the solutions used were left to stir overnight before spin-casting. To prepare a series of 11 polymer blend films with PI mass fraction Φ varying between 0 and 1, dPS (weight-average molecular weight $M_w = 174\,000$, polydispersity $M_w/M_n = 1.03$) and PI ($M_w = 400\,000$, $M_w/M_n = 1.12$) were used. For each fraction Φ, the films were cast (under identical conditions) onto hydrophobic and hydrophilic SAM substrates to form two series of samples. Deuterated polystyrene was used to provide contrast for ion beam techniques, which yield phase domain structure[50,52] related to surface patterns.

2.2. Surface Characterization. Topography of surface undulations formed in the course of spin casting was examined by the home-built[55] scanning force microscopy (SFM) working in contact mode.[23−24,33] All measurements were performed in air at room temperature. The cantilevers (purchased from Park Scientific Instruments), with Si_3N_4 tip, had a spring constant of ∼0.03 N/m. Tips were changed regularly to avoid artifacts due to tip contamination. Images with different scan range (from 2 μm × 2 μm to 30 μm × 30 μm) were recorded for each sample to illustrate best surface patterns and to provide data optimal for the Fourier transform analysis and the integral-geometry approach. The background due to the scanner tube movement is fully subtracted prior to analysis. Additional measurements of the blend films with $0.25 \le \Phi \le 0.45$ (i.e., for the surface patterns with large dominant length Λ) were performed with CP Park Scientific Instruments SFM working in contact mode[37−38,52] with maximum scan range (80 μm × 80 μm). As a result, statistically significant topographic data were always obtained.

To compare surface topography and the phase domain structure (determined in refs 50 and 52) with morphological measures, several lateral maps of domain distribution were obtained for the $\Phi = 0.40$ blend films cast on CH_3−SAM and COOH−SAM substrate. dPS composition maps were provided by the C_2D^- ($m/z = 26$) ions recorded with the imaging mode of dynamic SIMS.[50] SIMS compositional maps (typically with Rayleigh lateral resolution of ∼120 nm) were obtained with VSW apparatus equipped with high-resolution ion gun (double lens, liquid metal source, produced by Fei Company) and quadrupole mass spectrometer (Balzers) using a cylindrical mirror energy filter at the entrance.[50]

2.3. Image Analysis. Topographic (SFM) and compositional (SIMS) images were analyzed using the software developed in our laboratory.[37,38] To determine the dominant length Λ, 2-dimensional fast Fourier transform (FFT) of the studied image is computed. The FFT spectrum exhibits an isotropic diffusive ring. The radial average of the squared FFT amplitudes provides power spectrum $P(k)$ with the maximum positioned at the wave vector $k = 1/\Lambda$. The exact position of this peak (and its uncertainty) is determined from a fit of a Lorentz line shape to the $P(k)$.[37] For each image, a complete set of morphological measures was calculated (as described in section 3.2) using the algorithm of ref 44 (simpler but equivalent to that of ref 45, used previously[3]). Analysis of several images yields the Minkowski measures representative for each blend film. The Minkowski measures calculated for the large-scale structures of the surface morphologies with two lateral length-scales ($0.25 \le \Phi \le 0.45$) correspond to the images with all the surface features smaller than 10% of Λ neglected.[51]

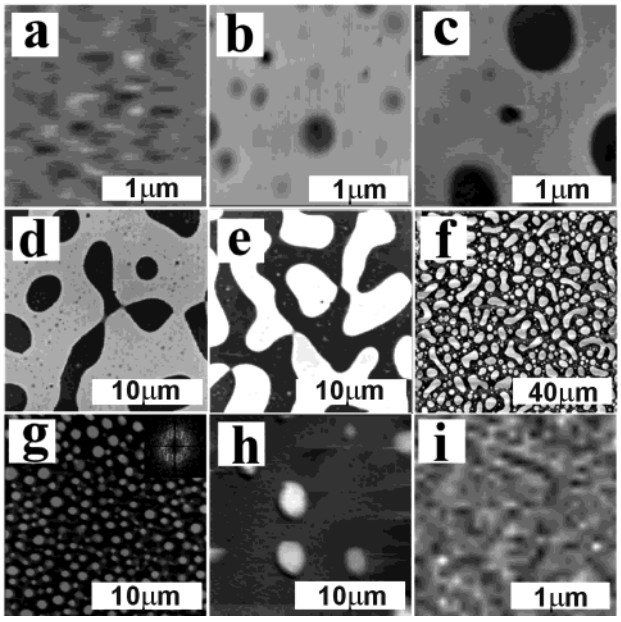

Figure 1. SFM images of surface patterns formed by polymer films of the dPS/PI series spin-cast on CH_3−SAM substrate for PI mass fraction $\Phi = 0$ (a), 0.05 (b), 0.15 (c), 0.25 (d), 0.4 (e), 0.45 (f), 0.6 (g), 0.85 (h), and 1.0 (i). Various scan ranges ($\Delta l \times \Delta l$) were used with $\Delta l = 2$ (a, b, c, i), 18 (d, e, g, h), and 80 μm (f). Different height ranges ΔH were applied to maximize the contrast. $\Delta H = 2.5$ (a), 25 (b), 80 (c), 105 (d), 185 (e), 220 (f), 135 (g), 74 (h)m and 2 nm (i). The inset in image g represents the FFT spectrum.

3. Results and Discussion

3.1. Surface Patterns (SFM) and Phase Domain Structure (SIMS). Representative surface morphologies, determined with SFM for polymer films cast on hydrophobic and hydrophilic SAM substrates, are collected in Figures 1 and 2, respectively. dPS (Figures 1a and 2a) and PI (Figures 1i and 2i) homopolymer films are fairly featureless (note the height range $\Delta H = 2-2.5$ nm used to illustrate statistical character of height fluctuations, discussed in section 3.2). In contrast, blending these polymers results in distinct surface patterns (here $\Delta H = 25-220$ nm), which evolve in a similar way for both types of the substrate with increasing PI blend composition Φ (Figures 1b−h and 2b−h). All the surface patterns formed for blend films are isotropic, as indicated by diffusive rings exhibited by FFT spectra of SFM images (see, e.g., insets to Figures 1g and 2g). At low Φ, hole-dominated morphologies are formed, characterized by a polymer sheet with polydisperse holes (Figures 1b,c and 2b,c). For higher Φ, surface coverage, perimeter, and depth of holes increase.

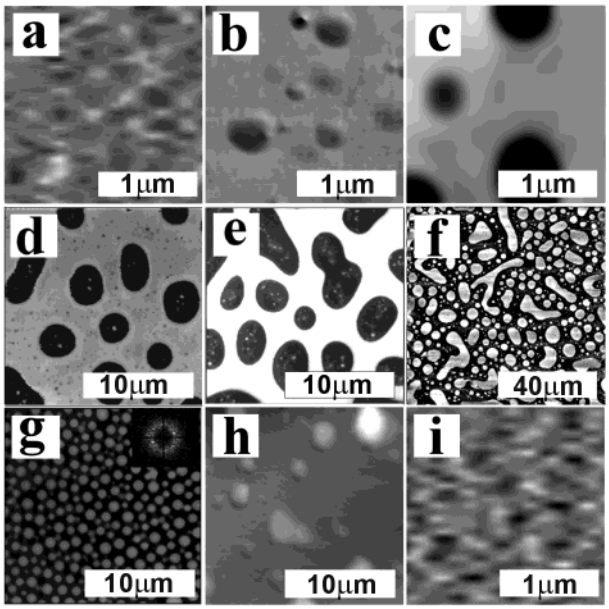

Figure 2. As for Figure 1 but for polymer films spin-cast on a COOH−SAM substrate.

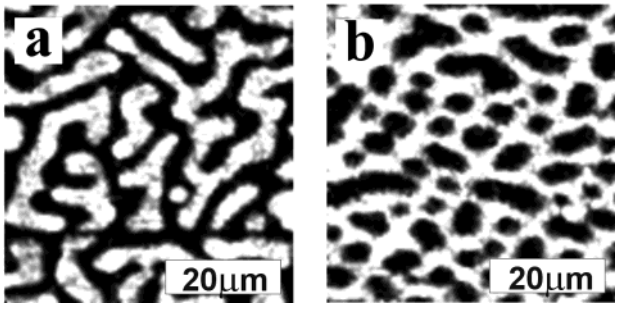

Figure 3. SIMS distribution maps (49 μm × 49 μm) of dPS recorded for the dPS/PI ($\Phi = 0.4$) blend film cast on CH_3−SAM (a) (cf. Figure 1e) and COOH−SAM (b) (cf. Figure 2e).

At fractions $\Phi = 0.25-0.45$, surface patterns with two dominant lateral length scales are formed, corresponding to elongated large-scale surface patterns and much smaller circular features (Figures 1d−f and 2d−f). The large-scale hole-dominated (nearly bicontinuous) structures are transformed into large-scale elongated protrusions at $\Phi \sim 0.36(3)$ and 0.42(2) for CH_3− and COOH−SAM substrates, respectively. Protrusions with two different length scales evolve, for higher Φ, into polydisperse circular islands with decreasing surface coverage, perimeter, and height (Figures 1g,h and 2g,h).

Phase domain structure of the studied blends were determined earlier, initially by a combination of SFM and selective dissolution of dPS and PI[24] and more precisely with imaging[50,52] and depth profiling[52] dynamic SIMS mode and X-ray photoelectron spectroscopy.[52] It has been shown[24,50,52] that the lateral domain structure corresponds to the patterns of surface undulations with elevated and depressed regions formed by dPS- and PI-rich phases, respectively. For instance, dPS-composition maps (see Figure 3) determined with dynamic SIMS for the $\Phi = 0.40$ blend films cast on CH_3−SAM and COOH−SAM correspond to large-scale elevations dominated by islands (cf. Figures 3a and 1e) and holes (cf. Figures 3b and 2e), respectively. This quasi-2-dimensional phase domain structure is positioned onto PI-rich lamella adjacent to the substrate.[24,52] It is also covered by a very thin (∼10 nm thick) PI layer.[50,52] A similar lateral phase arrangement was concluded earlier for another polystyrene (PS)/ PI system using selective dissolution and optical microscopy.[42−43] This technique was, however, unable to resolve vertical structure, surface undulations, and small domains.

The above-mentioned correspondence between surface patterns and lateral phase domain structure is then confirmed by rigorous analysis within integral-geometry approach (see section 3.2). This relation is a consequence of the phase separation occurring in the course of a three-step spin-casting process.[2,3,4,20,27] First, most of the homogeneous fluid (here composed of dPS and PI dissolved in toluene) is spun-off, leaving a uniform film. Second, radial flow of the fluid decreases film thickness. Preferential PI segregation to both external surfaces[14,56−57] (γ(PI) = 32 mJ/m^2 < γ(dPS) = 40 mJ/m^2) is followed by subsequent lateral phase separation (initiated by decreasing toluene concentration c_t and constrained to 2 dimensions by the film geometry).[52] Third, phase separation is terminated when c_t is so low that dPS molecules are no longer mobile (glass transition temperature T_g(dPS) = 100 °C, T_g(PI) = −70 °C). The lateral domain structure, although frozen in place, is reflected in surface undulations since the rate of solidification due to the solvent evaporation as well as the polymer swelling in the remaining toluene is different[20] for PI- and dPS-rich phases.[52] As a consequence, lateral dPS- and PI-rich domains are elevated and depressed, respectively.

The polymer/polymer interaction parameter between dPS and PI, $\chi = 0.034$,[57] yields the effective parameter value $2\chi/\chi_c = 81.2$ (χ_c is the χ value at the critical point) corresponding to the upper regions of weak incompatibility regime defined for ultrathin (i.e., with thickness $d \sim 2-4R_g$) blend films.[3] However, for thicker films, distinctive surface patterns are expected for whole composition window $0 \le \Phi \le 1$ even for blends with smaller effective $2\chi/\chi_c$ value.[1,20,22,35] Observed here surface patterns (Figures 1 and 2) reflect lateral domain structures with morphology dependent on blend composition[42] (similarly to two-phase morphologies formed due to temperature jump[58,59]). Droplet patterns, dominated by PI-rich (holes) and dPS-rich (islands) domains of the minority phase, correspond to off-critical compositions ($\Phi < 0.25$ and $\Phi > 0.45$, respectively). While ideal bicontinuous spinodal-type morphology is manifested for blends with Φ close to Φ_{cr} (when vertical phase rearrangement can be neglected[43]), a crossover to droplet pattern is expected for compositions shifted away from bulk critical composition Φ_{cr}.[59] As a result, nearly bicontinuous structures are formed. They are dominated by elongated holes or islands for lower or higher Φ values, respectively, from the composition range $0.25 \le \Phi \le 0.45$. In addition to the large-scale structures discussed above, the surface patterns observed for $0.25 \le \Phi \le 0.45$ are characterized also by much smaller features (Figures 1d−f and 2d−f). Such morphologies, reflecting phase arrangements with two length scales, indicate double quench scenario.[59−61] This phase separation pathway, characteristic for systems with intermediate viscosity and low diffusion coefficient,[60] was observed previously for other blend films.[20,38] Local compositions of large-scale elongated domains, formed by fast hydrodynamic process, are far from equilibrium values. Such domains exhibit secondary phase separation process resulting in additional much smaller, circular domains.[59] These two length scales are char-

acteristic for nearly bicontinuous spinodal morphologies[59,60] and are absent for nucleation-type surface patterns observed for off-critical blends[2,5,42] (here for $\Phi < 0.25$ and $\Phi > 0.45$).

3.2. Minkowski Measures of Individual Images. Topographic or compositional images of polymer blend films represent arrays of pixels set to a various gray level depending on the value of local height or composition. Each pixel can be reset to either white or black depending on whether its local value is larger or lower than the threshold variable. Using height or concentration as the threshold variable[45] each image is transformed into a series of black-and-white images (so-called level contours). Then the values of Minkowski functionals are determined for each level contour. Such a threshold procedure[45,47] results in the plots of the Minkowski measures against the threshold variable.

The Minkowski functionals are defined on homogeneous domains A.[19,46,47] Each domain A can be represented as a finite union of compact convex sets in d-dimensional space, for instance pixels in a black-and-white image. Any additive, motion invariant and conditional continuous functional $W(A)$ can be written in terms of the $(d + 1)$ Minkowski functionals $W_\nu(A)$.[19,46,47] In other words, the Minkowski functionals provide the complete set of morphological measures. In $d = 2$ space values of the Minkowski functionals are related to familiar measures: the covered (white) area $F = W_0$, the boundary length (perimeter) $U = 2W_1$, and the Euler characteristic $\chi_E = W_2/\pi$.[46−47] The Euler characteristic χ_E of a homogeneous domain is defined by the difference of the number of connected regions N_w (white) and the number of uncovered holes N_b (black), i.e., $\chi_E = N_w - N_b$.[19,46] Morphological content of each 2-dimensional level contour is described by the Minkowski measures (F, U, and χ_E), calculated for the whole black-and-white image, normalized additionally by the total analyzed area.[45−47] This normalization is necessary to provide easy comparison of the measures determined for images with different scan ranges.

Morphological Measures of Topographic Images. The threshold procedure is illustrated here for topographic images of polymer blend films. Height is here the threshold variable. Parts a−c of Figure 4 (parts d−f) show exemplary level contours transformed from SFM image of Figure 1e (2e) for three successive height values.

The values of the Minkowski measures determined for a series of level contours, corresponding to given topographic surface pattern, can be represented as the plots against threshold variable.[3] Characteristic features of such plots (Figure 5), computed for SFM images recorded for different types of surface morphologies, will be now discussed. We start with fairly featureless SFM image of flat homopolymer film (e.g., Figure 2a). Corresponding height relations of the Minkowski measures (dotted lines in Figure 5a−c) are symmetric, with the point (F, χ_E) or line (U) of symmetry specified by the average height $\langle h \rangle$ of the SFM image. Hyperbolic tangent and its derivatives describe well the measures (with $F = 0.5$, maximum U and $\chi_E = 0$ at height $\langle h \rangle$). In contrast to this case, with ideal monomodal height distribution, the surfaces of the blend films with $\Phi = 0.05$ (e.g., Figure 2b) or $\Phi \geq 0.85$ (e.g., Figure 1h) exhibit the distribution affected by holes or islands (see solid and dashed lines in Figures 5d−f), respectively. The plots are asymmetric and extended to heights lower (for holes, $\chi_E < 0$) or higher (for islands, $\chi_E > 0$) than the average value $\langle h \rangle$. All the other film surfaces ($0.15 \leq \Phi < 0.85$), dominated by holes (e.g., Figure 2e) or islands (e.g., Figure 1e), always exhibit bimodal height distribution (see solid and dashed lines in Figures 5a−c). In an ideal case the relations of the Minkowski measures characteristic for individual sheets, centered at two dominant height levels $\langle h_1 \rangle$ and $\langle h_2 \rangle$, are simply superposed. While this superposition is sometimes not observed for the height relations of boundary length U or the Euler characteristic χ_E[3], the plots of fractional area F can be always approximated by double hyperbolic tangent centered at $\langle h_1 \rangle$ and $\langle h_2 \rangle$.

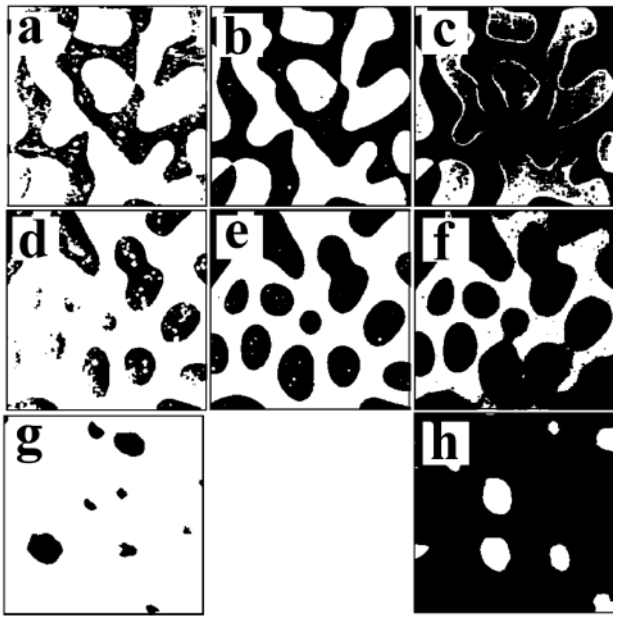

Figure 4. Black-and-white images (level contours) derived from SFM images shown in Figures 1e (a−c), 2e (d−f), 2b (g), and 1h (h). The threshold variable value is specified by the dominant height levels $\langle h_1 \rangle$ (a, d), $(\langle h_1 \rangle + \langle h_2 \rangle)/2$ (b, e), $\langle h_2 \rangle$ (c, f), $\langle h \rangle - 3w_F$ (g), and $\langle h \rangle + 3w_F$ (h) (see text for details).

For each SFM image, its characteristic morphological measures are specified by their values determined for the *representative level contour*. For surface morphologies with bimodal height distribution we define this representative black-and-white image as corresponding to the threshold variable $h = (\langle h_1 \rangle + \langle h_2 \rangle)/2$. As a result homogeneous black and white domains are obtained clearly resembling original SFM images (cf. Figures 4b and 1e and also Figures 4e and 2e). This definition is also supported by the fact that the measure F (and to a much smaller extent U or χ_E) remains almost constant for the region around $(\langle h_1 \rangle + \langle h_2 \rangle)/2$ (see Figure 5a−c), reflecting very steep boundaries of the holes or the islands. Uncertainty of this threshold value is given by the average width $\langle w_F \rangle$ characteristic for two hyperbolic tangents used to approximate the $F(h)$ relation. For the surface patterns with monomodal height distribution, we take the level contours determined for the heights $h = \langle h \rangle - 3w_F$ or $\langle h \rangle + 3w_F$ as representative for hole- or island-dominated morphologies, respectively. Height oscillations (see Figures 1a and 2a) of the sheet centered at $\langle h \rangle$ extend approximately to $h = \langle h \rangle \pm 2w_F$. Therefore, the proposed threshold heights (with uncertainty w_F) are the nearest to $\langle h \rangle$ possible values resulting in black (cf. Figures 4g and 2b) and white (cf. Figures 4h and 1h) domains best resembling the original SFM images.

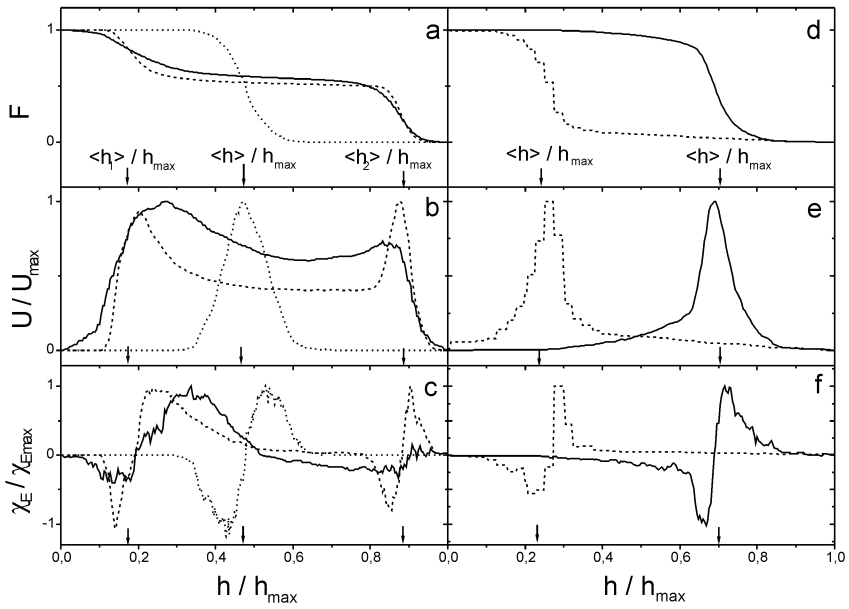

Figure 5. Minkowski measures (the area fraction F (a, d), the boundary length U (b, e) and the Euler characteristic χ_E (c, f)) of individual SFM images plotted as a function of the threshold height variable h. The relations are presented for five different types of surface patterns: fairly flat surface (Figure 2a) (dotted lines in a−c), surfaces with monomodal (Figures 2b and 1h) (d−f) and bimodal (Figures 2e and 1e) (a−c) height distribution dominated by holes (solid lines) or islands (dashed lines). Dominant height levels of monomodal ($\langle h \rangle$) and bimodal ($\langle h_1 \rangle$, $\langle h_2 \rangle$) distribution are marked. Maximum values of U, χ_E, and h are used to present a few relations on each plot.

We note also that height relations of the Minkowski measures can reflect[3] the specific shape of the elevated or depressed regions, visible directly in sectional views of SFM images. For instance, the concave shape of the elevations with rims higher than inner plateaus (Figure 4c, level contour determined for $\langle h_2 \rangle$) is reflected in the local maximum of U (dashed line in Figure 5b, extreme centered at $\langle h_2 \rangle$). In contrast to these observations made for the $\Phi = 0.4$ films on CH_3−SAM, the same local maximum is much weaker (solid line in Figure 5b) for the same blend films cast on COOH−SAM. This reflects the changed, now convex, shape of the elevations (cf. level contours of Figure 4, parts e and f, the latter determined for $\langle h_2 \rangle$). Substrate chemistry modifies here not only the shape of free surface profiles but also lateral phase domain structure (cf. Figure 4, parts b and e or Figure 3, parts a and b). The latter relation, manifested only for blend compositions Φ close to Φ_{cr}, will be discussed in the next section. These two effects have different origin, as demonstrated by symmetric ($\Phi = 0.50$) blend films,[24,52] where the substrate chemistry affects the shape of free surface elevations but not the lateral phase arrangement. The proposed[52] relevant mechanism involves formation and (subsequent) solidification of dPS-rich domains with substrate dependent curvature of their surface faces, followed by the collapse of PI-rich phase below the average height of the domains rich in dPS. In turn, the formation of convex (concave) surface faces of dPS-rich domains was reported to be related[52] with the observed faster (slower) toluene evaporation from the blend films positioned on COOH−SAM (CH_3−SAM).

Morphological Measures of Compositional Images. Comparison with the Measures of Topographic Images. The procedure used to determine the Minkowski measures characteristic for compositional map is similar to that described above for topographic images. The characteristic values of the Minkowski functionals are specified for representative level contour. It is simply provided by black-and-white image with fractional area F equal to the average concentration in the determined compositional map. Here, for the analyzed dPS compositional maps (Figure 3) of the films with $\Phi = 0.40$ known from preparation, we assume $F = 1 - \Phi = 0.6$.

Table 1. Minkowski Measures (Fractional Area F, Boundary Length U, Euler Characteristic χ_E) of the Large-Scale Structures Observed in Topographic (SFM) and Compositional (SIMS) Maps of the Films with PI Blend Composition $\Phi = 0.4$ Cast on CH_3−SAM and COOH−SAM Substrate[a]

substrate	CH_3−SAM	CH_3−SAM	COOH−SAM	COOH−SAM
map	SFM	SIMS	SFM	SIMS
F	0.55(6)	0.6 (fixed)	0.58(6)	0.6 (fixed)
U (μm^{-1})	0.62(2)	0.59(6)	0.64(1)	0.62(5)
χ_E (μm^{-2})	0.007(5)	0.005(5)	−0.041(7)	−0.026(9)

[a] The average values and random uncertainties, presented in four columns, correspond in each case to several maps analyzed.

As noticed earlier (in section 3.1) imaging SIMS mode can resolve the large-scale component of the phase domain structure with two length scales. The Minkowski measures of these large-scale structures, observed (at different spots of the same samples) in compositional maps and topographic[51] images are compared in Table 1. Within uncertainty ranges the measures of both data types accord with each other confirming the correspondence between surface topography and lateral phase domain structure, mentioned in section 3.1.

3.3. Analysis of the Surface Patterns Formed by Blend Films. The analysis of individual SFM images allows us now to present a cumulative description of two series of surface structures formed by the films with varied blend composition cast on two types of substrates. The lateral aspect of the surface morphologies is characterized by the Minkowski measures. A measure of the vertical extent Δh of the surface patterns can be also provided by the integral-geometry approach. For films with bimodal height distribution the extent Δh is simply specified by both dominant height levels ($\Delta h = \langle h_2 \rangle - \langle h_1 \rangle$). Only for the blend films with $\Phi = 0.05$ and $\Phi \geq$

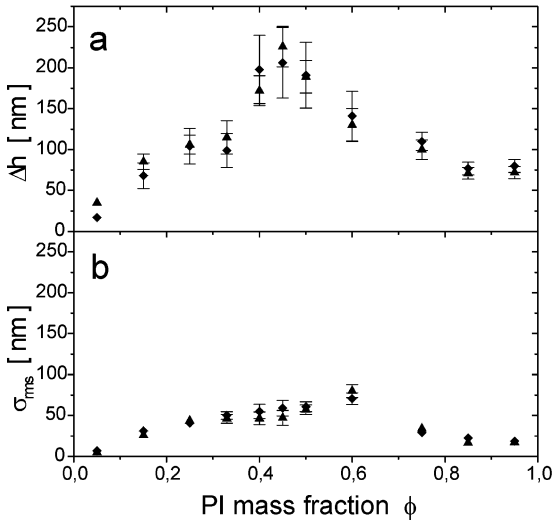

Figure 6. Vertical extent Δh (a) and roughness σ_{rms} (b) determined as a function of PI blend composition Φ for the surface patterns formed by the films cast on CH_3−SAM (triangles) and COOH−SAM (diamonds).

0.85, Δh is approximated by the average depth/ height determined from several sectional views of SFM images. Determined dependence of the vertical extent Δh as a function of PI blend composition Φ is presented in Figure 6a. The root-mean-square roughness σ_{rms} of the same surface patterns is plotted in Figure 6b. Both compositional relations are identical for blend films cast on CH_3−SAM as well as on COOH−SAM substrates (marked as triangles and diamonds, respectively). Significantly higher Δh values are observed for PI mass fractions $0.4 \leq \Phi < 0.6$.

The Minkowski measures are plotted in Figure 7 as a function of PI blend composition Φ for films prepared on CH_3−SAM (data denoted as triangles) and COOH−SAM (data denoted as diamonds and squares). Figure 7a represents the values of fractional area F compared with the dependence, marked as a solid line, corresponding to the linear relation between surface coverage F of elevated (dPS-rich) domains and dPS volume fraction. Such a simple relation between surface coverage by one of the immiscible blend components and its volume fraction is expected for the quasi-2-dimensional system realized by a thin film confined by symmetric neutral flat surfaces.[13,14,62] Factors affecting this relation, connected with the formation of dPS-rich protrusions at the free surface and PI-rich lamella at the substrate, seem to neutralize each other. As a consequence, the accord between the data and the curve (Figure 7a) is observed, confirming the earlier outlined (section 3.1) scenario of the spin-casting process, where 2-dimensional phase separation plays an important role. Surface topographic patterns are formed as the solidification rate as well as the polymer swelling in toluene is different for (drying) PI- and dPS-rich domains of the 2-dimensional phase-separated structures. Both volume effects would be maximal for symmetric (50% v/v) blends, i.e for $\Phi = 0.47$ in accord with the observed extreme of vertical extent Δh (see Figure 6a).

The boundary length U of the surface patterns is plotted in Figure 7b as a function of PI blend composition. Almost identical relations are observed for films on CH_3−SAM and COOH−SAM. The Euler characteristic of the same patterns is shown in Figure 7c. To present all the data in a convenient way we have plotted

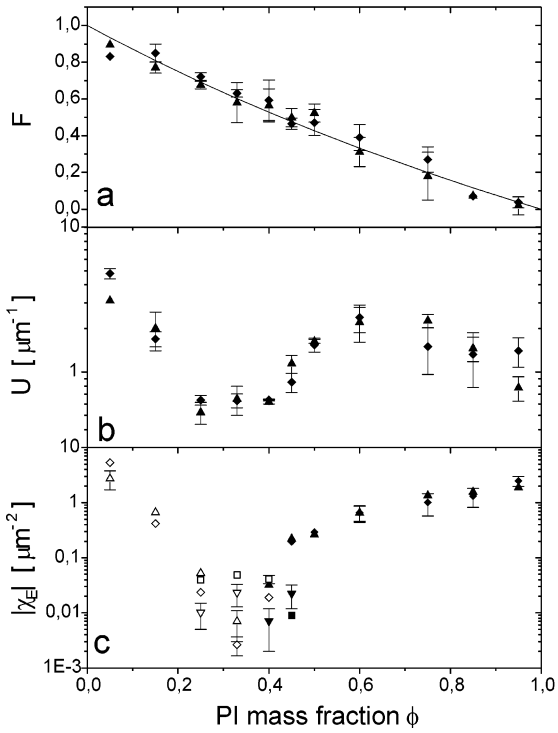

Figure 7. Minkowski measures (the area fraction F (a), the boundary length U (b), and the Euler characteristic χ_E (c)) of the surface patterns formed by the films with different PI blend composition Φ. The solid line in part a corresponds to a linear relation between F and the dPS volume fraction. Positive and negative values of the measures are marked by solid and open symbols, respectively. Up-triangles (for CH_3−SAM) and diamonds (for COOH−SAM) correspond to all features of the surface patterns. Down-triangles (for CH_3−SAM) and squares (for COOH−SAM) correspond to the morphologies with small-scale features neglected ($0.25 \leq \Phi \leq 0.45$, patterns with two length scales).

only absolute values $|\chi_E|$, but marked them as open and solid symbols for $\chi_E < 0$ and $\chi_E > 0$, respectively. The χ_E data points, reflecting all the features of the surface patterns for films deposited on CH_3−SAM and COOH−SAM, are marked as up-triangles and diamonds, respectively. In addition, for fractions $0.25 \leq \Phi \leq 0.45$ (morphologies with two length scales), the χ_E values determined for the morphologies with small-scale features neglected are denoted as down-triangles (CH_3−SAM) and squares (COOH−SAM). We observe an overall correspondence between the plots showing the density of boundary length U (Figure 7b) and the effective density of continuous features χ_E (Figure 7c). It reflects the fact that the main factor influencing total boundary length is the number of the features. Feature size seems to play a role only for extreme ($\Phi \rightarrow 0$ and $\Phi \rightarrow 1$) blend compositions. The morphological measure χ_E, presented in Figure 7c, reflects the topology of formed surface patterns very well. Surface morphologies with very high density of features are formed for compositions $\Phi < 0.25$ and $\Phi > 0.45$. In turn, blend films with $0.25 \leq \Phi \leq 0.45$ are described by a region of minimal values of effective density of features $|\chi_E|$. For this composition range the elongated large-scale structures were observed (see section 3.1). At characteristic compositions Φ_{h-i}, $\chi_E \rightarrow 0$ corresponding to ideal bicontinuous morphology. Hole-dominated ($\chi_E < 0$, open symbols in Figure 7c) nearly bicontinuous structures are transformed into large-scale elongated islands ($\chi_E > 0$, solid symbols) at $\Phi_{h-i} \sim 0.36(3)$ and 0.42(2) for CH_3−

SAM and COOH−SAM, respectively. These values are close to the bulk critical weight fraction $\Phi_{cr} = 0.34$ of the binary dPS/PI mixture. The same value Φ_{cr} is expected for thin films with symmetric neutral flat walls.[13,14,62] The effects due to vertical phase rearrangement are relevant also here. However, they result effectively only in small and dependent on polymer/substrate interactions[42,43] shifts of Φ_{h-i} with respect to Φ_{cr}.

3.4. Analysis of Individual Dominant Features of the Surface Patterns. Dominant features of the surface patterns correspond to holes and islands, for negative and positive χ_E values, respectively. For the morphologies with two length scales dominant features are specified by the large-scale structures.[63] The individual dominant surface feature is characterized by the average area S and the mean radius of its boundaries r_C:

$$S = \begin{cases} (1 - F)/\chi_E; & \chi_E < 0 \\ F/\chi_E; & \chi_E > 0 \end{cases} \quad (1)$$

$$r_C = U/(2\pi\chi_E) \quad (2)$$

both specified by the relevant[63] Minkowski measures. Plots of the absolute values of these measures against PI blend composition Φ are presented in Figure 8, parts a and b. Data points are marked as in Figure 7c, i.e., with open and solid symbols for negative (holes) and positive (islands) values, respectively. The transformation from hole- into island-dominated structures (at fraction Φ_{h-i}) is accompanied by maximum values of the average area $|S|$ (and the mean radius $|r_C|$) observed for the islands formed right after the transformation (i.e., at $\Phi = 0.40$ for CH_3−SAM and 0.45 for COOH−SAM). Region of ideal bicontinuous morphology, with $|S|$ diverging to very high values, was analyzed previously with optical microscopy.[42,43]

The $|S|$ values extend over 3 orders of magnitude, with lateral length scales spanned from hundreds of nanometers (for extreme blend compositions $\Phi \to 0$ and $\Phi \to 1$) to a few micrometers (this distinct behavior is observed for the films with $0.25 \le \Phi < 0.45$). Composition dependence of the average area $|S|$ of individual (dominant) surface feature (Figure 8a) resembles that one of the mean radius $|r_C|$ (Figure 8b) except the more pronounced region of high values of the latter. The reason for this behavior is the characteristic, and constant for some blend compositions, shape of individual surface features. The circular character of individual features is characterized by the parameter $|r_C|/[|S|/\pi]^{1/2}$, plotted against PI mass fraction in Figure 8c. The constant and close to 1 value of this parameter for off-critical blend films with nucleation-type surface morphologies (i.e., for $\Phi < 0.2$ and $\Phi \ge 0.5$) should be noticed. In contrast, the $|r_C|/[|S|/\pi]^{1/2}$ values are almost 1 order of magnitude larger for the range $0.25 \le \Phi \le 0.45$, indicating spinodal-type structures with elongated dominant surface features.

The Minkowski measures can be also used to define lateral length scales complementary to the dominant length Λ. The Λ values (see Figure 9a), determined with the Fourier transform analysis, correspond to the radial averaged wavelength of dominant surface undulations. However, the distance between individual dominant surface features can be also estimated (somewhat more roughly) by the measure $1/|\chi_E|^{1/2}$, i.e., the mean distance occupied by each feature (Figure 9b). It turns out that

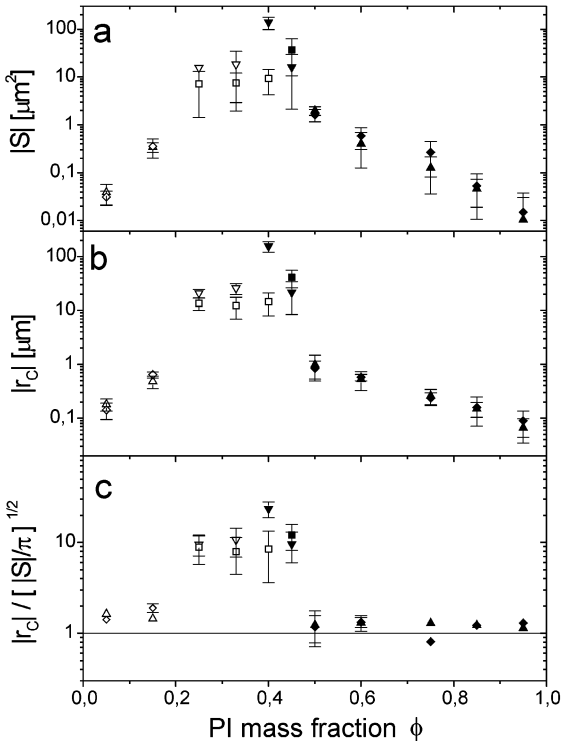

Figure 8. Average area S (a) and mean radius r_C (b) of individual dominant features of the surface patterns plotted against PI blend composition Φ. The circular character of the individual features is measured by the parameter $r_C/(|S|/\pi)^{1/2}$ (c), equal to 1 (solid line) for ideal circular features. Symbols are as in Figure 7.

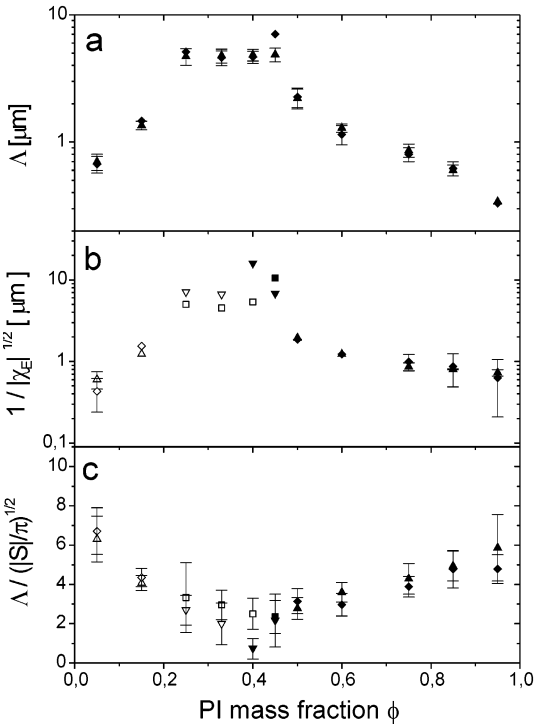

Figure 9. Dominant length Λ (a) of the surface pattern, determined with the Fourier transform analysis, compared with complementary length scales, such as the mean distance occupied by one individual dominant surface feature $1/|\chi_E|^{1/2}$ (b) and the mean lateral extent $(|S|/\pi)^{1/2}$ of each feature. The ratio $\Lambda/(|S|/\pi)^{1/2}$ is plotted in part c. Symbols are as in Figure 7.

$1/|\chi_E|^{1/2}$ provides a reasonable estimation of Λ (cf. Figure 9, parts a and b, with an average $\Lambda|\chi_E|^{1/2}$ value of 0.88-

(6)). In Figure 9c the distance Λ between individual (dominant) surface features is compared with mean lateral extent of each feature defined by $(|S|/\pi)^{1/2}$. We observe that the separation Λ of the dominant features is comparable to their lateral extent only for nearly bicontinuous morphologies but becomes a few times higher than $(|S|/\pi)^{1/2}$ for extreme blend compositions ($\Phi \rightarrow 0$ and $\Phi \rightarrow 1$).

4. Summary and Conclusions

The presented extension of the integral-geometry approach provides morphological measures on three different levels: (a) for individual images (section 3.2), (b) for a series of surface patterns (formed by various blend films, section 3.3), and (c) for individual (dominant) features of these patterns (section 3.4).

The amount of information given by morphological measures allows us to perform a thorough characterization impossible with the parameters used earlier (such as dominant length Λ determined with the Fourier transform analysis). (a) Using height h or concentration Φ as the threshold variable, each image is transformed into a series of (black-and-white) level contours, characterized by the area fraction F (coverage), the boundary length U (lateral shape) and the Euler characteristic χ_E (connectivity) of the (white) features. The Minkowski measures (F, U, χ_E) plotted against height reflect different surface topography types (fairly flat surfaces, hole- or island- dominated surfaces with mono- and bimodal height distribution) and specific shapes (sharp-edged or round) of free surface profiles. The height relations are used to determine vertical extent Δh of the surface pattern and its characteristic (lateral) measures (F, U, χ_E). In turn, the Minkowski measures of the compositional images are provided by the level contours specified by blend composition Φ. Analysis of several images yields the parameters (F, U, χ_E and Δh for SFM data) characteristic for each blend film. (b) Compositional relations of the vertical extent Δh and the Minkowski measures determine composition ranges and transitions between different morphologies (e.g., dominated by holes, $\chi_E < 0$, islands, $\chi_E > 0$, or nearly bicontinuous structures with minimal $|\chi_E|$ values). (c) Finally, the Minkowski measures are used to define morphological measures of an individual dominant surface feature, such as its average area S, the mean radius r_C, the mean lateral extent $(|S|/\pi)^{1/2}$, the measure $|r_C|/[|S|/\pi]^{1/2}$ of circular character, and the mean occupied distance $1/|\chi_E|^{1/2}$. These measures specify properties (and composition ranges) of different morphologies (e.g., droplet patterns with $|r_C|/[|S|/\pi]^{1/2} \sim 1$, and nearly bicontinuous structures with large $|S|$ values).

The integral-geometry approach is demonstrated here for two series of model films of the dPS/ PI mixture, cast from toluene on Au substrates covered with hydrophobic or hydrophilic SAM. Information available with this approach verifies hypotheses[1,5,20,22,27,42,52] on film morphology formation. (a) Height relations of the Minkowski measures reflect fairly featureless surfaces for pure polymer films and distinct surface features for the blends. This indicates that the surface patterns are formed as a consequence of phase separation enabled by the solvent.[20,42] The correspondence between surface patterns and lateral phase domain structure is confirmed rigorously by the comparison of the Minkowski measures. This suggests that the surface pattern replicates[1,20,22,27,52] the (formed earlier) lateral phase arrangement. (b) The relevant mechanism[20,52] related to volume effects (solidification rate and extent of swelling in toluene different for both phases) is verified by the extreme Δh values observed for symmetric and nearly symmetric compositions. In addition, only for the (nearly) symmetric blends the effects of substrate-dependent shape of free surface profiles[52] are detected, resulting in the specific $U(h)$ relations. Quasi-2-dimensional character[42] of the formed lateral phase structures is reflected in the $F(\Phi)$ relation. Vertical phase rearrangement effects[22,27] result only in a small substrate dependent[42] composition shift of the region with ideal bicontinuous morphology (visible in the $\chi_E(\Phi)$ plot). (c) The compositional relations plotted for the Minkowski measures (U, χ_E) and related parameters ($|S|$, r_C, $r_C/(|S|/\pi)^{1/2}$, $1/|\chi_E|^{1/2}$) specify composition ranges of various morphologies, most probably related with different types of lateral phase separation.[5,42,59,64] The distance Λ between the surface features, defined rigorously by Fourier analysis, is well estimated by $1/|\chi_E|^{1/2}$. This is true also for nucleation-type morphologies[64] with Λ few times higher than the mean lateral extent $(|S|/\pi)^{1/2}$ of each surface feature.

The virtues of the integral-geometry approach are presented here for dominant surface features, which are equivalent to large-scale structures for the patterns with two length scales. Cumulative analysis of large- and small-scale surface features, discussed for an another system in our previous work,[38] can provide a test for the models[3,20,59] describing double quench scenario for phase separation of polymer films in the course of spin-casting.

Acknowledgment. We are grateful to the members of Prof. R. Hołyst's group for useful discussions. One of us (J. Raczkowska) acknowledges with appreciation a W. Trzebiatowski scholarship. We thank Prof. M. Szymoński for the access to the SFM apparatus at Joint Center for Chemical Analysis and Structural Research of the Jagellonian University. This work was partially supported by the Reserve of the Rector of the Jagellonian University.

References and Notes

(1) Tanaka, K.; Takahara, A.; Kajiyama, T. *Macromolecules* **1996**, *29*, 3232−3239.
(2) Affrossman, S.; Henn, G.; O'Neill, S. A.; Pethrick, R. A.; Stamm, M. *Macromolecules* **1996**, *29*, 5010−5016.
(3) Gutmann, J. S.; Müller-Buschbaum, P.; Stamm, M. *Faraday Discuss.* **1999**, *112*, 258−297.
(4) Budkowski, A.; Bernasik, A.; Cyganik, P.; Rysz, J.; Brenn, R. *e-Polymers* **2002**, *006*, 1−21.
(5) Ermi, B. D.; Karim, A.; Douglas, J. F. *J. Polym. Sci., Part B: Polym. Phys.* **1998**, *36*, 191−200.
(6) Wang, H.; Composto, R. J. *Europhys. Lett.* **2000**, *50*, 622−627.
(7) Hoppe, H.; Heuberger, M.; Klein, J. *Phys. Rev. Lett.* **2001**, *86*, 4863−4866.
(8) Nakai, A.; Shiwaku, T.; Wang, W.; Hasegawa, H.; Hashimoto, T. *Macromolecules* **1996**, *29*, 5990−6001.
(9) Nakai, A.; Wang, W.; Ogasawara, S.; Hasegawa, H.; Hashimoto, T. *Macromolecules* **1998**, *31*, 5391−5398.
(10) Hayashi, M.; Ribbe, A.; Hashimoto, T.; Weber, M.; Heckmann, W. *Polymer* **1998**, *39*, 299−308.
(11) Ribbe, A. E.; Hayashi, M.; Weber, M.; Hashimoto, T. *Polymer* **1998**, *39*, 7149−7151.
(12) Krausch, G. *Mater. Sci. Eng.* **1995**, *R14*, 1−94.
(13) Binder, K. *Adv. Polym. Sci.* **1999**, *138*, 1−89 and references therein.
(14) Budkowski, A. *Adv. Polym. Sci.* **1999**, *148*, 1−111 and references therein.

(15) Geoghegan, M.; Krausch, G. *Prog. Polym. Sci.* **2003**, *28*, 261−302.
(16) Walheim, S.; Schäffer, E.; Mlynek, J.; Steiner, U. *Science* **1999**, *283*, 520−522.
(17) Arias, A. C.; MacKenzie, J. D.; Stevenson, R.; Halls, J. J. M.; Inbasekaran, M.; Woo, E. P.; Richards, D.; Friend, R. H. *Macromolecules* **2001**, *34*, 6005−6013.
(18) Moons, E. *J. Phys.: Cond. Matter* **2002**, *14*, 12235−12260.
(19) Mecke, K. R. *Int. J. Mod. Phys. B* **1998**, *9*, 861−899.
(20) Walheim, S.; Böltau, M.; Mlynek, J.; Krausch, G.; Steiner, U. *Macromolecules* **1997**, *30*, 4995−5003.
(21) Walheim, S.; Ramstein, M.; Steiner, U. *Langmuir* **1999**, *15*, 4828−4836.
(22) Ton-That, C.; Shard, A. G.; Teare, D. O. H.; Bradley, R. H. *Polymer* **2001**, *42*, 1121−1129.
(23) Rysz, J.; Ermer, H.; Budkowski, A.; Lekka, M.; Bernasik, A.; Wróbel, S.; Brenn, R.; Lekki; J.; Jedliński, J. *Vacuum* **1999**, *54*, 303−307.
(24) Bergues, B.; Lekki, J.; Budkowski, A.; Cyganik, P.; Lekka, M.; Bernasik, A.; Rysz, J.; Postawa, Z. *Vacuum* **2001**, *63*, 297−305.
(25) Chen, C.; Wang, J.; Woodcock, S. E.; Chen, Z. *Langmuir* **2002**, *18*, 1302−1309.
(26) Ade H.; Winesett, D. A.; Smith, A. P.; Qu, S.; Ge, S.; Sokolov, J.; Rafailovich, M. *Europhys. Lett.* **1999**, *45*, 526−532.
(27) Sprenger, M.; Walheim, S.; Budkowski, A.; Steiner, U. *Interface Science* **2003**, *11*, 225−235.
(28) Sung, A.; Karim, A.; Douglas, J. F.; Han, C. C. *Phys. Rev. Lett.* **1996**, *76*, 4368−4371.
(29) Heier, J.; Kramer, E. J.; Revesz, P.; Battistig, G.; Bates, F. S. *Macromolecules* **1999**, *32*, 3758−3765.
(30) Müller-Buschbaum, P.; O'Neill, S. A.; Affrossman, S.; Stamm, M. *Macromolecules* **1998**, *31*, 5003−5009.
(31) Gutmann, J. S.; Müller-Buschbaum, P.; Schubert, D. W.; Stribeck, N.; Stamm, M. *J. Macromol. Sci.—Phys. B* **1999**, *38*, 563−576.
(32) Müller-Buschbaum, P.; Gutmann, J. S.; Stamm, M. *Macromolecules* **2000**, *33*, 4886−4895.
(33) Rysz, J.; Ermer, H.; Budkowski, A.; Bernasik, A.; Lekki, J.; Juengst, G.; Brenn, R.; Kowalski, K.; Camra, J.; Lekka, M.; Jedliński, J. *Eur. Phys. J. E* **2001**, *5*, 207−219.
(34) Müller-Buschbaum, P.; Gutmann, J. S.; Stamm, M. *J. Macromol. Sci.—Phys. B* **1999**, *38*, 577−592.
(35) Müller-Buschbaum, P.; Stamm, M. *Colloid Polym. Sci.* **2001**, *279*, 376−381.
(36) Ermi, B. D.; Nisato, G.; Douglas, J. F.; Rogers, J. A.; Karim, A. *Phys. Rev. Lett.* **1998**, *81*, 3900−3903.
(37) Cyganik, P.; Bernasik, A.; Budkowski, A.; Bergues, B.; Kowalski, K.; Rysz, J.; Lekki, J.; Lekka, M.; Postawa, Z. *Vacuum* **2001**, *63*, 307−313.
(38) Cyganik, P.; Budkowski, A.; Raczkowska, J.; Postawa, Z. *Surf. Sci.* **2002**, *507−510*, 700−706.
(39) Affrossman, S.; Stamm, M. *Colloid Polym. Sci.* **2000**, *278*, 888−893.
(40) Affrossman, S.; Jerome, R.; O'Neill, S. A.; Schmitt, T.; Stamm, M. *Colloid Polym. Sci.* **2000**, *278*, 993−999.
(41) Affrossman, S.; O'Neill, S. A.; Stamm, M. *Macromolecules* **1998**, *31*, 6280−6288.
(42) Dalnoki-Veress, K.; Forrest, J. A.; Stevens, J. R.; Dutcher, J. R. *J. Polym. Sci., Part B: Polym. Phys.* **1996**, *34*, 3017−3024.
(43) Dalnoki-Veress, K.; Forrest, J. A.; Stevens, J. R.; Dutcher, J. R. *Physica A* **1997**, *239*, 87−94.
(44) Michielsen, K.; De Raedt, H. *Phys. Rep.* **2001**, *347*, 461−538 and references therein.
(45) Mecke, K. R. *Phys. Rev. E* **1996**, *53*, 4794−4800.
(46) Mecke, K. R.; Sofonea, V. *Phys. Rev. E* **1997**, *56*, R3761−R3764.
(47) Sofonea, V.; Mecke, K. R. *Eur. Phys. J. B* **1999**, *8*, 99−112.
(48) Aksimentiev, A.; Moorthi, K.; Hołyst, R. *J. Chem. Phys.* **2000**, *112*, 6049−6062.
(49) Fialkowski, M.; Aksimentiev, A.; Holyst, R. *Phys. Rev. Lett.* **2001**, *86*, 240−243.
(50) Bernasik, A.; Rysz, J.; Budkowski, A.; Kowalski, K.; Camra, J.; Jedliński, J. *Macromol. Rapid Commun.* **2001**, *22*, 829−834.
(51) The morphological measures were calculated for the original representative level contour (for definition see section 3.2) with all the domains smaller than 10% of Λ removed. This procedure practically does not affect either the measure F (see Figure 7) or the threshold height defining the representative level contour.
(52) Budkowski, A.; Cyganik, P.; Bernasik, A.; Raczkowska, J.; Penc, B.; Bergues, B.; Kowalski, K.; Janik, J. *Macromolecules*, submitted for publication.
(53) Genzer, J.; Kramer, E. J. *Phys. Rev. Lett.* **1997**, *78*, 4946−4949.
(54) Böltau, M.; Walheim, S.; Mlynek, J.; Krausch, G.; Steiner, U. *Nature* **1998**, *391*, 877−879.
(55) Lekki, J.; Voss, U.; Sowa, M.; Cleff, B.; Stachura, Z. Report No. 1690/AP; Institute of Nuclear Physics: Kraków, Poland, 1995.
(56) Hasegawa, H.; Hashimoto, T. *Polymer* **1992**, *33*, 475−487.
(57) Budkowski, A.; Klein, J.; Steiner, U.; Fetters, L. J. *Macromolecules* **1993**, *26*, 2470−2478.
(58) Bates, F. S. *Science* **1991**, *251*, 898−905.
(59) Tanaka, H. *Phys. Rev. E* **1995**, *51*, 1313−1329 and references therein.
(60) Wagner, A. J.; Yeomans, J. M. *Phys. Rev. Lett.* **1998**, *80*, 1429−1432.
(61) Hayashi, M.; Jinnai, H.; Hashimoto, T. *J. Chem. Phys.* **2000**, *112*, 6897−6909.
(62) Rouault, Y.; Dünweg, B.; Baschnagel, J.; Binder, K. *Polymer* **1996**, *37*, 297−304.
(63) For $0.25 \leq \Phi \leq 0.45$, small-scale (secondary) structures are neglected to exclude any effects of bimodal lateral length distribution.
(64) Tanaka, H.; Yokokawa, T.; Abe, H.; Hayashi, T.; Nishi, T. *Phys. Rev. Lett.* **1990**, *65*, 3136−3139.

MA020870W